Obstructed Diffusion in Phase-Separated Supported Lipid Bilayers: A Combined Atomic Force Microscopy and Fluorescence Recovery after Photobleaching Approach

Timothy V. Ratto* and Marjorie L. Longo*†

*Biophysics Graduate Group, Division of Biological Sciences, and †Department of Chemical Engineering and Material Science, University of California, Davis, Davis, California 95616 USA

ABSTRACT Proteins and other macromolecules are believed to hinder molecular lateral diffusion in cellular membranes. We have constructed a well-characterized model system to better understand how obstacles in lipid bilayers obstruct diffusion. Fluorescence recovery after photobleaching was used to measure the lateral diffusion coefficient in single supported bilayers composed of mixtures of 1,2-dilauroylphosphotidylcholine (DLPC) and 1,2-distearoylphosphotidylcholine (DSPC). Because these lipids are immiscible and phase separate at room temperature, a novel quenching technique allowed us to construct fluid DLPC bilayers containing small disk-shaped gel-phase DSPC domains that acted as obstacles to lateral diffusion. Our experimental setup enabled us to analyze the same samples with atomic force microscopy and exactly characterize the size, shape, and number of gel-phase domains before measuring the obstacle-dependent diffusion coefficient. Lateral obstructed diffusion was found to be dependent on obstacle area fraction, size, and geometry. Analysis of our results using a free area diffusion model shows the possibility of unexpected long-range ordering of fluid-phase lipids around the gel-phase obstacles. This lipid ordering has implications for lipid-mediated protein interactions in cellular membranes.

INTRODUCTION

Cell membrane structure has gone through several refinements since 1925 when Gorter and Grendel (1925) first proposed lipid bilayers. The bilayer structure was seen as serving as a barrier to molecular transport from the medium containing a cell into the cell interior. The largest paradigm shift occurred in the 1970s when biologists began to consider the biological importance of lateral diffusion and the possibility of molecular interactions within the plane of the membrane itself. This was formally expressed in the conceptual fluid mosaic model of Singer and Nicholsen (1972) that envisioned a cell membrane as a two-dimensional oriented viscous solution of integral proteins uniformly distributed in a homogeneous fluid matrix. More recent studies have shown that cell membranes are not the homogeneous structures that were originally predicted. It now seems obvious that neither lipids nor proteins are randomly distributed within the plane of the membrane (Abney and Scalettar, 1995; Brown and London, 2000; Bussell et al., 1994; Gheber and Edidin, 1999; Harroun et al., 1999; Johnson et al., 1996; Simson et al., 1998). This nonrandom distribution appears to be important for cell function (Ho et al., 1992; Ladha, 1998) and so a greater understanding of how molecules diffuse in inhomogeneous membranes is necessary to understand, for example, membrane pathologies that result in cell dysfunction (Ditaranto et al., 2001; Eze, 1992; Owen, 1990).

The fundamental question concerning lateral diffusion in cell membranes is why diffusion coefficients for both protein and lipid diffusion in cell membranes are often orders of magnitude slower than diffusion coefficients measured in model systems (Webb et al., 1981; Cherry et al., 1998; Picard et al., 1998). Much has been learned recently about retardation of diffusion in cell membranes, and it has become known that in many cells, confinement zones of up to several microns in diameter restrict diffusion. The existence of these zones has been attributed to diffusing particles encounters with a membrane skeleton fence (Sako and Kusumi, 1995) with relatively fast diffusion within the fence but longer-range diffusion restricted by barriers between zones. Even within these zones, however, the fast diffusion rates are slower than rates observed in pure lipid bilayers, indicating that another mechanism must be playing a role in the restriction of diffusion. Additionally, cells that contain little or no cytoskeleton still display slower diffusion in comparison with pure lipid bilayers (Kucik et al., 1999). It has been proposed that proteins and lipid inhomogeneities embedded within cellular membranes also act as obstacles to diffusion, and this is why lateral motion is slower than predicted (Minton, 1989; Almeida et al., 1992a). Another possibility is that rapid and repetitive transient binding and release from either slow-moving or immobile structures results in the diffusional decrease (Abney et al., 1989; Garver et al., 1997). Most likely, it is a combination of these mechanisms and as yet undiscovered mechanisms that are truly responsible. Fully understanding one of these proposed mechanisms, obstacle-mediated obstructed diffusion in the case of this study, will aid in developing an understanding of what is truly responsible for hindered diffusion in cellular membranes.

Submitted May 30, 2002, and accepted for publication July 16, 2002.

Address reprint requests to Dr. M. L. Longo, 3108 Bainer Hill, One Shields Ave., Davis, CA 95616-5294. Tel.: 530-754-6348; Fax: 530-752-1031; E-mail: mllongo@ucdavis.edu.

0006-3495/02/12/3380/13 $2.00

The relationships between lateral molecular distribution in membranes and lateral diffusion of lipids or proteins have been investigated experimentally and theoretically by a wide variety of techniques (Cherry et al., 1998; Feder et al., 1996; Gheber and Edidin, 1999; Johnson et al., 1996; Martins and Melo, 2001; Ladha, 1998; Minton, 1989; Picard et al., 1998). Among them Monte Carlo simulations have provided the clearest conceptual view of how diffusion is affected by the presence of obstacles (Pink et al., 1986; Saxton, 1989; Scalettar and Abney, 1991). However, direct comparison between simulation and experiment is difficult because of assumptions made within the simulations that are necessary for speed or convenience of programming. Other theoretical approaches have included hydrodynamic (Bussell et al., 1995; Dodd et al., 1995) and free-volume (Schram et al., 1994; Tocanne et al., 1994; Almeida et al., 1992b) theories. The former are suitable for analyzing protein diffusion but work poorly when modeling lipid diffusion (Vaz et al., 1985). Experimental data support the idea that diffusion of lipids follows the free-volume model, mainly because lipid diffusion has been shown to be independent of acyl chain length (Balcom and Petersen, 1993). This is in disagreement with hydrodynamic theories that include a strong diffusing particle-length-dependence term. One likely free-volume model for accurately predicting how obstacles should affect lipid diffusion was formalized by Almeida et al. in 1992 (Almeida et al., 1992a). In this model, Almeida et al. generalized the free-volume theory of lateral diffusion to a heterogeneous membrane in which immobile circular obstacles are assumed to be surrounded by a few layers of more highly ordered fluid lipids (compared with the bulk fluid) that serve to restrict diffusion. This soft-core repulsive model supercedes the original hard-core repulsive models and adds an additional parameter for understanding how obstacles in membranes reduce diffusion. The ordering of fluid lipids around integral membrane proteins is now well established (Harroun et al., 1999; Heller et al., 2000); however, although the Almeida model establishes limits for the order parameter, adding this component to the free-area models effectively creates a free parameter that has been used to help fit experimental data (Almeida et al., 1992a; Schram et al., 1994). Because of our unique experimental system we are able to unequivocally determine all parameters in this free-area model, including the order parameter, and thereby determine the suitability of this model for predicting diffusive behavior.

To construct an obstructed bilayer system, we used a mixture of two lipids that are immiscible at room temperature. It has previously been shown that gel-phase domains can act as obstacles to diffusion (Almeida et al., 1992a); however, these studies used calorimetry to estimate the amount, size, shape, and areas of the coexisting solid and fluid phases and were unable to determine whether the gel-phase domains were mobile in the fluid bilayer or immobile. Monte Carlo simulations have demonstrated that mobile obstacles restrict diffusion quite differently than immobile ones (Saxton, 1990). Here, we present direct atomic force microscopy (AFM) measurements of immobile gel domain sizes, shapes, and area fractions in phase-separated bilayers and show how the rate of diffusion in these bilayers is decreased by the presence of these gel-phase domains. We would like to emphasize that we do not claim that restriction of diffusion in actual cellular membranes is caused by the presence of gel-phase lipid. In our model system the gel-phase domains take the place of actual obstacles in cellular membranes, most likely proteins and protein aggregates, and/or regions of increased lipid order such as the hypothesized lipid rafts. However, it is expected that in membranes that contain proteins, additional protein-protein and protein-lipid interactions may prevent the direct application of simple diffusion models. We present the next logical experimental step in understanding how obstacles affect lateral diffusion in bilayers by investigating a simplified obstructed membrane that contains only lipids. Future research will include proteins, both as obstacles and as the diffusing species.

MATERIALS AND METHODS

Materials

1,2-Dilauroylphosphotidylcholine (DLPC), 1,2-distearolyphosphotidylcholine (DSPC), and 1-palmitoyl-2-[-6[{7-nitro-2–1,3-benzoxadiazol-4-yl} amino]caproyl]-*sn*-glycero-3-phosphatidylcholine)) (DC_{14}-NBD-PC) were purchased in chloroform from Avanti Polar Lipids (Birmingham, AL) and used without further purification. Small unilamellar vesicles were prepared using tip sonication (Branson sonifier, model 250, Branson Ultrasonics, Danbury, CT) of a 0.5 mg/ml lipid suspension. This method of resuspension and sonication is the same as described in McKiernan et al. (1997), except that a final sonication was used to heat the vesicles to ~70°C before placing the vial containing the small unilamellar vesicle solution into a 70°C water bath. All water used in these experiments was purified in a Barnstead Nanopure System (Barnstead Thermolyne, Dubuque, IA), with resistivity = 17.9 MΩ and pH 5.5.

Sample preparation

Vesicles were prepared from mixtures of DLPC/DSPC and contained a 1 mol % concentration of the fluorescent probe NBD-PC. Because this probe prefers to partition into the fluid DLPC areas (Mesquita et al., 2000), as we increased the amount of DSPC in our samples we decreased the amount of probe to maintain a 1 mol % concentration relative to the fluid phase. For all samples, a 150-μl droplet of the 70°C vesicle solution was added to a freshly cleaved room-temperature mica disk glued to a small metal puck as described previously (McKiernan et al., 2000). This quenching process has been shown to result in the formation of small lipid domains (Giocondi et al., 2001). The vesicle droplet was allowed to incubate on the mica disk for 30 min and then rinsed 10 times with purified water with a final liquid volume of ~200 μl. The sample was incubated for an additional 120 min to ensure that phase separation of the two lipids was complete before acquiring data.

AFM imaging

Samples were imaged with a Digital Instruments NanoScope IIIa (Santa Barbara, CA) in contact mode with either a J or E scan head. Sharpened,

coated AFM microlevers, model MSCT-AUHW (Park Scientific, Sunnyvale, CA) with nominal spring constants between 0.01 and 0.06 N/m were used for all scans. Hydration of the samples during scanning was maintained using Digital Instruments AFM tapping mode fluid cell, model MMTFC. Force scans were performed before imaging, and set points and scan rates were established in such a way as to minimize the force between the AFM tip and the sample. Usually, the set points ranged between 0.1 and 0.25 V with scan rates typically between 5 and 8 Hz. After imaging, the sample was removed from the AFM sample stage and placed in a small petri dish filled with purified water. Hydration of the bilayer was maintained at all times during the transfer of the sample. The petri dish containing the sample was then moved into the fluorescence recovery after photobleaching (FRAP) apparatus for diffusion measurements. We used the public domain software package Imagetool (University of Texas Health Science Center, San Antonio, TX), which can detect and measure physical parameters of the height images produced from the Digital Instruments AFM software, to analyze the size, shape, and area fraction of the solid-phase domains in our samples.

FRAP

FRAP experiments were carried out on a modified Nikon Eclipse 400 fluorescence microscope (Nikon, Melville NY). A 100-W xenon lamp was used as the fluorescence source. The full spectrum output of the lamp was sent through an infrared filter (Edmund Scientific, Barrington, NJ), through an iris that allows control of the size of the bleached area, and through a ×60 water immersion objective that had been focused onto the fluorescently labeled bilayer. The bleach spot size could be varied between ~20 and 200 μm in diameter, although most measurements were carried out at a bleach spot diameter of 60 μm. The bleaching time was always less than 10% of the half-time to full recovery to fulfill the mathematical requirement of an infinite reservoir of fluorescent probe molecules (this is necessary to apply the fitting equation described below). After bleaching, the lamp output was attenuated ×400 with neutral density filters and sent through a filter that allows excitation of the NBD-PC molecule at a wavelength of 488 nm. The fluorescence emission of the sample was collected by the ×60 water immersion objective, sent through a filter that eliminates the excitation light, and collected by a ×20 objective that focuses the filtered light onto a 100-μm pinhole (Edmund Scientific, Barrington, NJ). The spatially filtered light was then collected into a ×50 extra long working distance objective (Nikon) and finally focused onto the 200-μm^2 active area of a Perkin-Elmer Avalanche photo diode (APD; Perkin-Elmer, Wellesley, MA). The APD emits one 2.5-V TTL pulse for every ~10^4 photons that are detected. The pulses were counted by a Nanonics photon counter (Nanonics Ltd. Malcha, Jerusalem, Israel) and binned by a Perkin-Elmer lock-in amplifier (Perkin-Elmer). The signals were typically binned at 20 ms for the shorter recovery times and 500 ms for the longer recoveries. The APD signal was sent over a serial line into a personal computer and collected in an Excel spreadsheet where fluorescent intensity was graphed versus time to generate a recovery curve. The diffusion coefficient of the sample was measured by fitting the recovery curve with a solution to the differential equation for lateral transport of a molecule by diffusion (Axelrod et al., 1976), by the method of Soumpasis (1983). The instrument was calibrated and the fits verified with a mixture of PBS buffer and glycerol containing fluorescent fluorescein probe molecules (Periasamy and Verkman, 1998). Microliter solution volumes of these calibration mixtures were sandwiched between two glass coverslips to produce aqueous layers of uniform thickness, ~5 μm. The diffusion coefficients for these samples could be directly calculated from the viscosity of the mixture and were known from previous experiments (Periasamy and Verkman, 1998). For each lipid mixture, FRAP recoveries were run without a bleaching pulse to determine whether any photobleaching was occurring because of the attenuated observation beam. For all observation times below ~2000 s, bleaching from the observation light was less than 10% of the total recovery values. An additional control was suggested by Dan Axelrod (Univ. of Michigan, private communication, 2001) whereby the time to half-recovery for a fully fluid DLPC bilayer was measured with four increasing bleach spot sizes, 20, 50, 80, and 100 μm in diameter. If recovery of the bleach spot was determined only by diffusion of the probe molecules, a linear relationship between bleach spot size and recovery times should be observed, with the time to half-recovery going to zero at an extrapolated bleach spot size of zero. If other factors were leading to recovery of probe fluorescence, such as auto recovery of the probe molecule, a nonzero half-time to recovery will be seen. Measurements made on a DLPC bilayer containing 1 mol % NBD-PC showed that a small number of probe molecules were recovering spontaneously leading to an error of ~±0.03 in our measurements. This error has been added as *y*-axis error bars in all graphs showing diffusion coefficients.

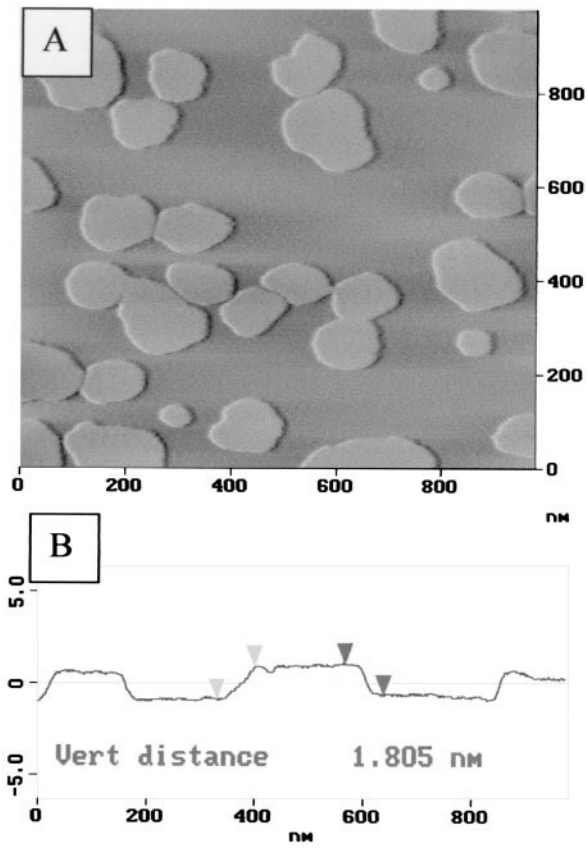

FIGURE 1 (*A*) A 900 × 900-nm AFM subtracted height-deflection image (chosen because it displays high contrast between the phases) of a mica-supported DLPC/DSPC bilayer containing 1 mol % NBD-PC relative to the fluid phase. Lighter colors denote higher areas. This sample was quenched from 70°C to 25°C, resulting in the formation of disk-shaped DSPC domains surrounded by a fluid DLPC bilayer. (*B*) AFM section analysis showing the ~1.8-nm height difference between the two phases.

RESULTS

General AFM results

Fig. 1 *A* shows a subtracted height/deflection (used to show greater contrast between phases) image of a supported bilayer formed through quenched vesicle fusion, containing a mixture of DLPC/DSPC and 1 mol % NBD-PC relative to

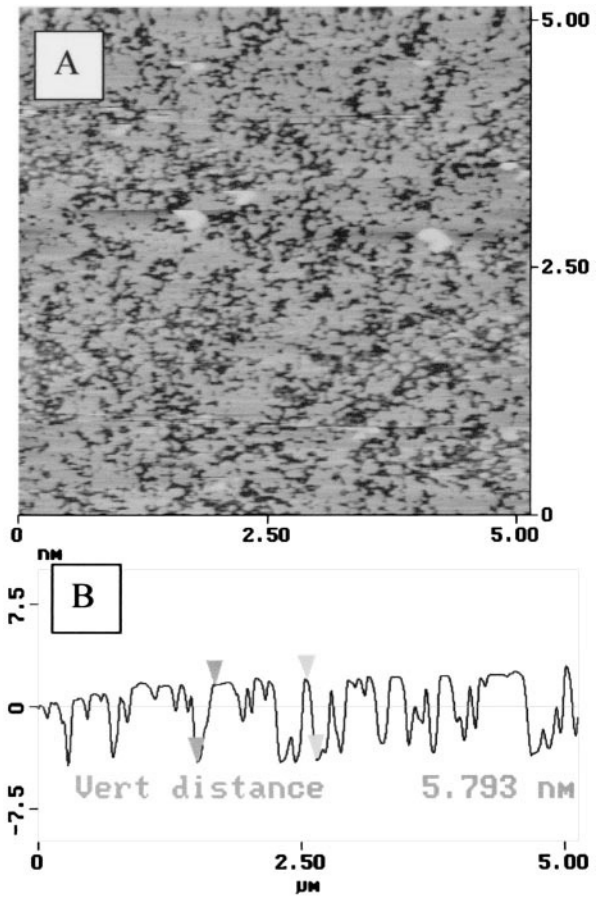

FIGURE 2 (*A*) A 5 × 5-μm AFM height image of a mica-supported DSPC bilayer displaying many defects; (*B*) The defects allow us to measure the thickness of the DSPC bilayer, ~5.8 nm. Assuming a 1-nm-thick water layer between the substrate and the bilayer results in a bilayer thickness of ~4.8 nm.

the fluid phase. The heated vesicles were deposited on a cooled mica substrate and thermal quenching from 70°C to 25°C resulted in phase separation of the solid lipid from the fluid lipid. The image illustrates how bilayers prepared in this manner contain relatively centrosymmetric DSPC domains extending from the DLPC matrix with a measured height difference of ~1.8 nm between the phases (Fig. 1 *B*). The domains are roughly monodispersed in size with the majority ranging between 40 and 70 nm in radius. Estimating an area of 45 Å^2 for an individual DSPC molecule suggests that each domain contains approximately between 10^5 and 10^6 lipid molecules. The DLPC/DSPC bilayers showed no defects or holes; however, a pure DSPC bilayer showed many defects that were ~5.8 nm deep (Fig. 2). Using this measurement as the height of the gel-phase lipid, we can calculate the thickness of the fluid phase by subtracting the 1.8-nm height difference between the phases from the 5.8-nm height of the gel-phase bilayer alone. This results in a measurement of 4.0 nm for the thickness of the fluid phase. Small-angle neutron scattering experiments have shown that a DLPC bilayer should be ~3.6 nm thick and a DSPC bilayer ~4.4 nm thick (Balgavy et al., 2001). The discrepancy between the small-angle neutron scattering data and our own is probably due to the existence of an ~1-nm water layer between the substrate and the multicomponent bilayer. Subtracting the height of the water layer from our measurements results in actual thicknesses of 3.0 and 4.7 nm for the DLPC and DSPC bilayer, respectively. Although the thickness measurement of the more rigid DSPC bilayer is most likely accurate, the fluid-phase DLPC bilayer is probably being compressed by the AFM tip, resulting in a decreased apparent thickness. In any case, these values are consistent with earlier reported values (Hollars and Dunn, 1998, 1997; McKiernan et al., 2000). We can increase the number of domains without significantly changing their size by increasing the proportion of DSPC in our DLPC/DSPC vesicles. Fig. 3 shows three AFM images with increasing numbers of domains and therefore increasing area fractions of the solid phase.

We call this sample preparation technique quenched vesicle fusion to distinguish the process from standard vesicle fusion techniques. In standard vesicle fusion, lipid vesicles are added to a substrate, with both the lipids and the support at the same temperature. In quenched vesicle fusion, vesicles consisting of mixtures of lipids are heated until the vesicle is a single-phase system. The solution of multi-lipid single-phase vesicles is then added to a support that is cooler than the vesicles. This results in the formation of a two-phase supported bilayer with phase separation not at equilibrium (Giocondi et al., 2001). By regulating the temperature differential between the vesicles and the support, the two-phase bilayer can be frozen at different points on the way to an equilibrium phase separation.

Larger temperature differentials between our DLPC/DSPC vesicles and the mica support (i.e., fast cooling rates) result in the formation of smaller DSPC domains whereas slower cooling rates lead to larger domains (Fig. 4), in keeping with previously reported phase behavior in lipid domains (McKiernan et al., 2000). Although a recent paper in this journal showed that complete phase separation for quenched DLPC/DSPC bilayers took place over time scales of hours (de Almeida et al., 2002), the DSPC domains in our supported bilayers did not change size or shape 30 min after quenching and were stable for 3 days after formation. An additional aspect of this stability was that the domains were relatively immobile. By acquiring images over several days we were able to detect a very slow mobility (~10–100 nm/h), but it was difficult to separate this effect from the thermal drift of our instrument. In any event, the domains were immobile over the time course of both our topographic and diffusional measurements. This immobility is presumably because the solid phase domains are too large to be moved by the thermally excited fluid lipid molecules.

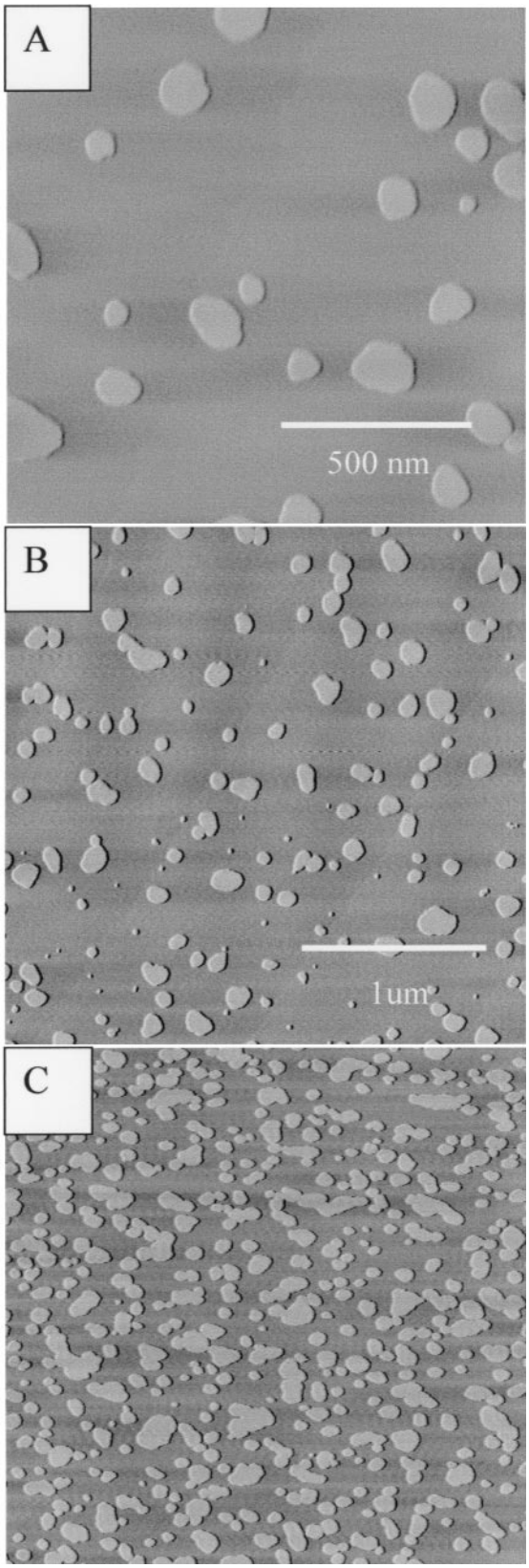

FIGURE 3 AFM subtracted height-deflection images of mica-supported DLPC/DSPC bilayers containing 1 mol % NBD-PC relative to the fluid phase at increasing area fractions of DSPC. These samples were quenched from 70°C to 25°C and contain ~15% (*A*), 25% (*B*), and 50% (*C*) gel-phase DSPC. Note that what appear to be very small domains are actually unfused vesicles.

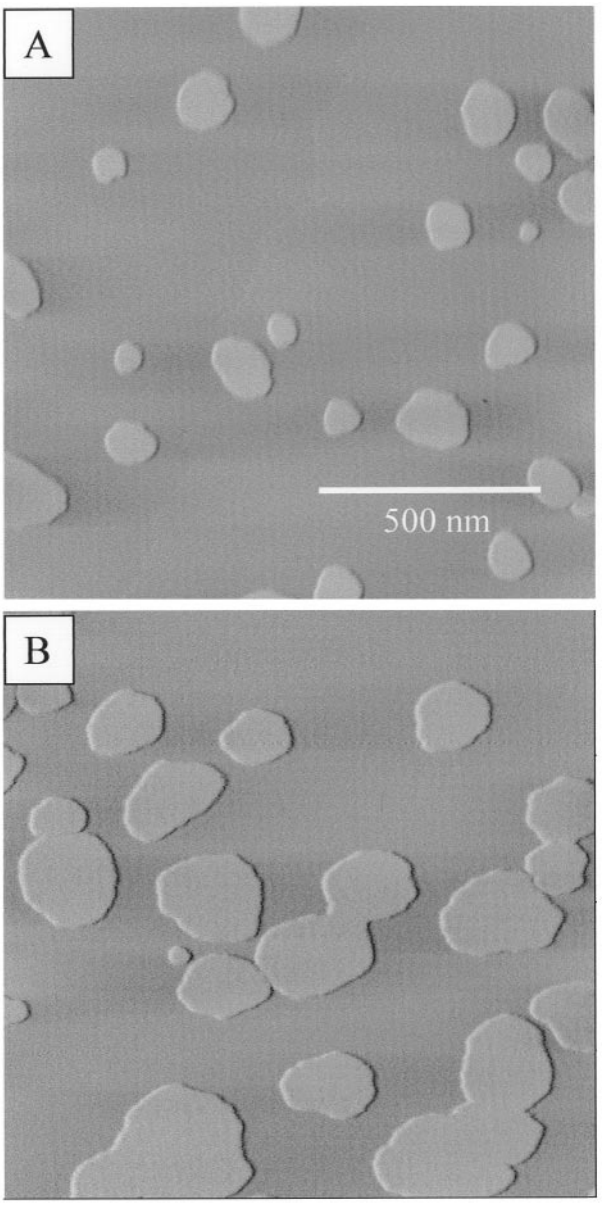

FIGURE 4 AFM subtracted height-deflection images of mica-supported DLPC/DSPC bilayers containing 1 mol % NBD-PC relative to the fluid phase. (*A*) A bilayer cooled from 70°C to 25°C; (*B*) A bilayer cooled from ~55°C to 25°C.

Size monodispersity and aggregation

Monte Carlo simulations have shown that obstacle size can have a large effect on how much the obstacles are able to hinder diffusion (Saxton, 1989, 1994, 1997). Because of this we were interested in defining exactly what our domain size range was and whether or not it was changing as we increased the ratio of DSPC to DLPC. Acquiring multiple

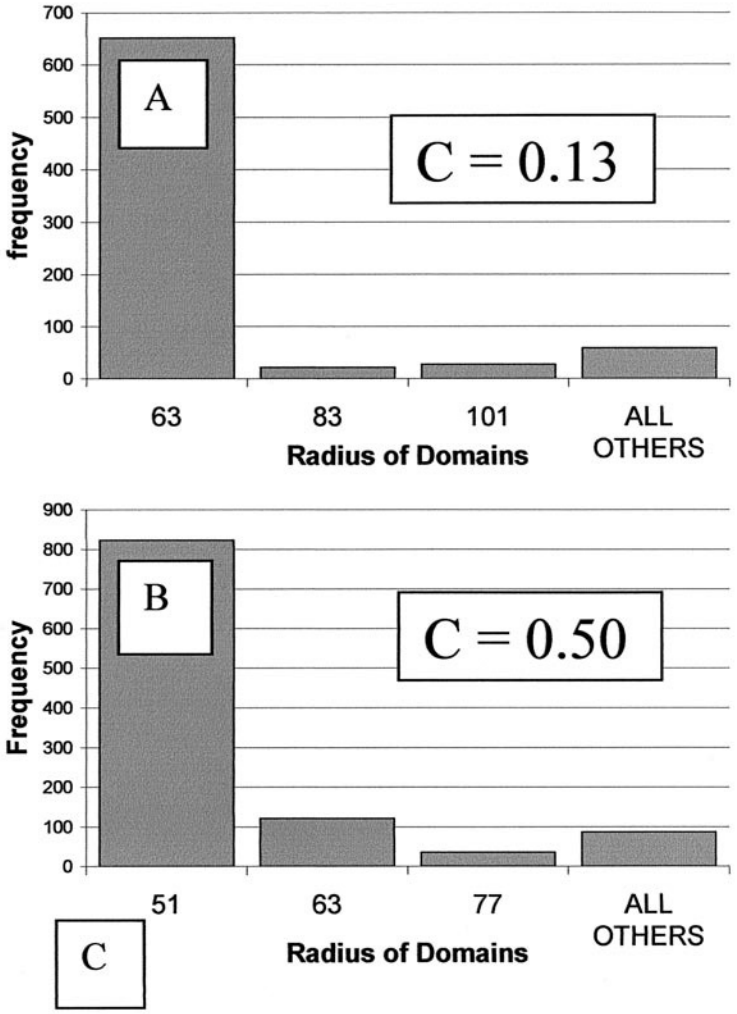

FIGURE 5 (*A* and *B*) Histograms of the size distribution of domain radii at two different area fractions of the solid phase; the numbers in the *x* axis refer to the center of a range 20 nm wide. The ALL OTHERS bin contains all other domain sizes not explicitly listed. (*C*) The percentage of total gel-phase area contained within the most frequently occurring domains for increasing area fractions.

Area Fraction (C)	Radius of Domain (R)	% Total gel-phase area enclosed
0.13	53-73 nm	83%
0.15	45-65 nm	81%
0.33	38-58 nm	76%
0.50	41-61 nm	74%

images for each sample and analyzing the size distribution allowed us to construct the histograms shown in Fig. 5. At lower gel-phase concentrations the majority of the gel domains range in size between 53 and 73 nm in radius and make up 83% of the total gel-phase area. As the concentration of gel phase increases, the domains get slightly smaller, ranging now from 41 to 61 nm and making up 74% of the total gel-phase area at an area fraction of 50%. The decrease in the total gel-phase area is attributed to aggregation of domains at higher area fractions. The size range shift from an average of 63 nm to an average of 51 nm is probably because of domain growth being constrained by the presence of barriers to diffusion in the form of gel-phase domains that are already present in the bilayer. Averaging the highest-frequency domain sizes for every area fraction gives an average radius of ~60 nm for all samples measured.

Some aggregation is present at all area fractions but accelerates once the area fraction increases beyond 50%. At this point the smaller domains come close enough together that they begin to aggregate and form clusters (Fig. 6). As

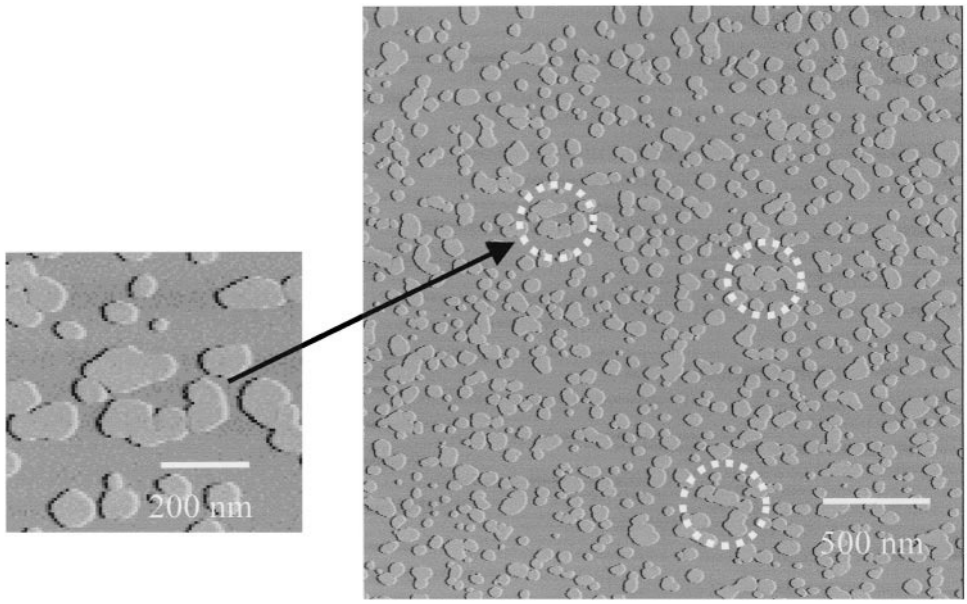

FIGURE 6 AFM subtracted height-deflection image of a mica-supported DLPC/DSPC bilayer at a DSPC area fraction of ~50%. The insert shows aggregation and the formation of extended rather than compact domains. These extended domains are more efficient than the compact disk-shaped domains at restricting diffusion.

we continue to increase the area fraction of gel-phase lipid, aggregation continues and the fluid-phase areas decrease in size until they are disconnected at an area fraction of ~70% (Fig. 7 *A*) and form separate pools of fluid-phase lipid. Continuing to increase the relative proportion of DSPC to DLPC results in the additional decrease in the size of the DLPC pools. The area fraction of solid phase at which disconnection of the fluid phase and consequent connection of the solid phase occurs is known as the percolation threshold (Lee and Torquato, 1990; Almeida et al., 1992a). We can determine this point in our DLPC/DSPC bilayers by assessing the total length of all fluid-phase areas within the sample. The point at which the length of the longest fluid path becomes smaller than the width of the image (defined as 5 μm in our studies) is the percolation threshold. It can be argued that we are assessing only the threshold at which a 5-μm area becomes discontinuous; however, larger scans as well as the FRAP data reported in the next section also indicate that the fluid phase becomes discontinuous at an area fraction of ~70%. Increasing the area fraction of DSPC past the percolation threshold resulted in an additional decrease of the fluid-phase areas (Fig. 7 *B*).

FRAP results

Fig. 8 shows some typical fluorescence recovery curves acquired from bilayers consisting of mixtures of DLPC and DSPC. When the bilayer consists solely of DLPC (Fig. 8 *A*), recovery is fast and complete. As the bilayer contains increasing amounts of gel-phase DSPC, and thus higher area fractions of the solid phase, diffusion becomes increasingly hindered. At high concentrations of DSPC, above area fractions of ~60% solid phase, diffusion is highly restricted and fluorescence recovery does not go to completion. This indicates that many of the fluid areas are already disconnected and therefore inaccessible to replenishment by unbleached probe molecules. Fluorescence recovery is abolished at an area fraction of ~70% solid-phase lipid, in agreement with the AFM data, implying that the fluid phase has become disconnected from the solid phase and the percolation threshold has been reached. Fig. 8 *B* shows a typical normalized recovery curve and an analytical fit of the recovery equation to the curve. Table 1 shows diffusion coefficients for supported lipid bilayers containing increasing ratios of DLPC/DSPC determined by fitting the analytical equation to our recovery data. These values are within the range of 1–10 $\mu m^2/s$ seen in other bilayer systems (Periasamy and Verkman, 1998; O'Toole et al., 1999; Schwille et al., 1999; Korlach et al., 1999).

We were also interested in how the size of the gel-phase domains influenced diffusion. We analyzed diffusion in a variety of samples that displayed the same area fraction of solid-phase lipid but contained different size domains. We are able to control the final size of our gel-phase domains by controlling the quenching rate, and so we could measure diffusion in bilayers containing obstacles with radii ranging between 40 and 130 nm. At a constant area fraction of 33%, smaller obstacles were more efficient than larger obstacles at hindering diffusion (Fig. 9). This effect has been reported from Monte Carlo simulations of diffusion as well as in protein aggregation experiments (Schram et al., 1994; Saxton, 1989). According to our data, this effect decreases with increasing obstacle size and becomes fairly constant when the obstacle radii increase above ~100 nm. Heating a previously phase-separated bilayer to 37°C and cooling very slowly to room temperature caused the many small gel-phase domains to segregate into a small number of very large domains (~2–3 μm) that maintained the same approx-

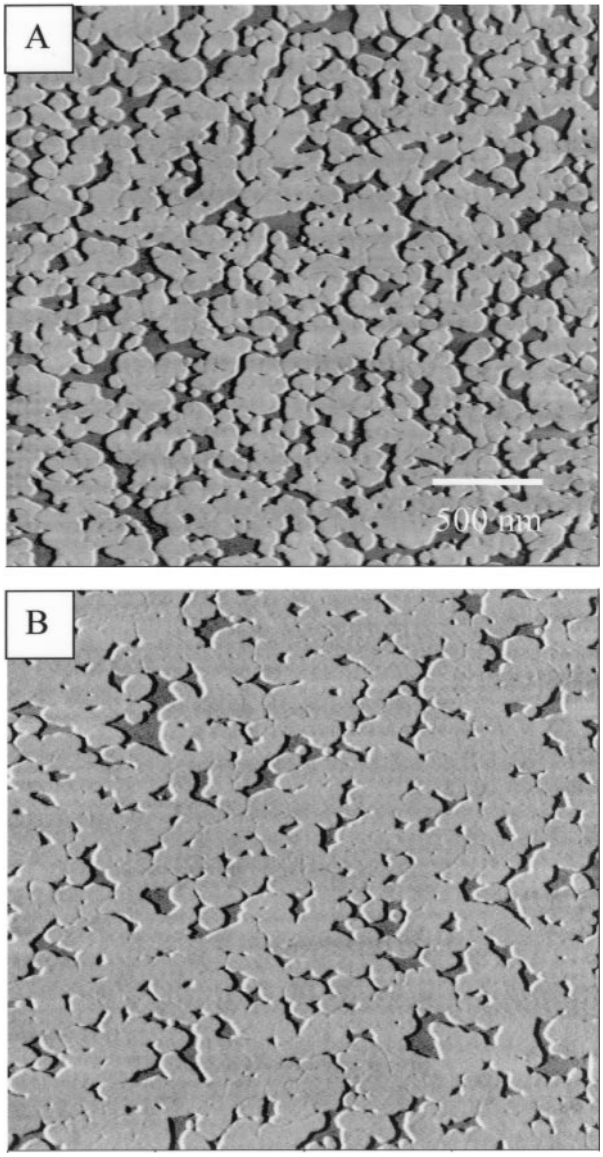

FIGURE 7 AFM subtracted height-deflection images of mica-supported DLPC/DSPC bilayers at gel-phase area fractions higher than the percolation threshold. (*A*) The DLPC/DSPC bilayer at the percolation threshold, the point at which the fluid-phase lipid becomes discontinuous and is confined in pools; (*B*) As the ratio of DSPC to DLPC increases, the fluid-phase pools decrease in size.

imate gel-phase area fraction of the bilayer before heating. Diffusion coefficients measured in this and similarly prepared samples were very close to rates measured in pure fluid bilayers, indicating that the large domains were unable to obstruct diffusion.

DISCUSSION

Percolation

The connectivity of obstructed systems is systematically treated in percolation theory. At low obstacle concentrations the obstacles form islands in the connected conducting phase. As the concentration of islands is increased, they eventually connect and separate the conducting phase to form pools in a continuous obstructed phase, the point at which this occurs is called the percolation threshold. Note that in lipid bilayer percolation analysis, the threshold is given in terms of the area fraction of obstacles; in the physics literature, it is more often given in terms of the area fraction of the conducting phase (Vaz, 1992). The percolation threshold has been found to be geometry dependent, with the area fraction of obstacles necessary to cut off the conducting phase increasing with increasing compactness (e.g., decreasing perimeter/area) of the obstacles. Thus, overlapping disk-shaped obstacles, which can form irregular extended geometries, percolate at an area fraction of 0.676, whereas nonoverlapping disks percolate at an area fraction of 0.82 (Berryman, 1983; Lee and Torquato, 1990). These two geometries are of particular importance for our system of quenched DLPC/DSPC. Correlating the AFM data with the FRAP data indicates that the long-range diffusion coefficient goes to zero at an area fraction of ~0.70, meaning that percolation is abolished at this area fraction, as predicted by the AFM results alone. According to continuum percolation theory (Lee and Torquato, 1990) this indicates that our system is behaving like a percolating system made of circular obstacles that can overlap. A more surprising result is shown in Fig. 10, where we have graphed the relative diffusion coefficient $\langle D \rangle$ versus area fraction (C). $\langle D \rangle$ is simply a ratio of the diffusion coefficient in a system containing obstacles (D) to diffusion in a fully fluid system (D_o). What is immediately apparent is that two diffusion regimes exist, characterized by two different slopes. This is unexpected because most theoretical treatments of diffusion in thin films predict a linear decrease in diffusion with increasing area fraction of obstacles. Additional analysis of the AFM data gives us the answer; at area fractions greater than 50%, aggregation of the gel phase domains occurs and leads to the formation of extended domains (Fig. 11). Extended obstacles have been shown to be more efficient than compact obstacles in hindering diffusion because of confinement of the conducting phase (Schram et al., 1996; Saxton, 1992).

An extrapolation of the $\langle D \rangle$ versus C data down to the x axis for area fractions less than 0.5 shows that the percolation threshold for this system would occur at an area fraction of ~0.8. This is quite close to the percolation threshold for a system of nonoverlapping disks and is additional evidence to support the idea that before aggregation the obstacles are indeed restricting diffusion as disks.

Free-area models

Free-area lipid diffusion models attempt to determine a rate-limiting step for diffusion and then model the simplified rate-limiting process analytically. This approach is

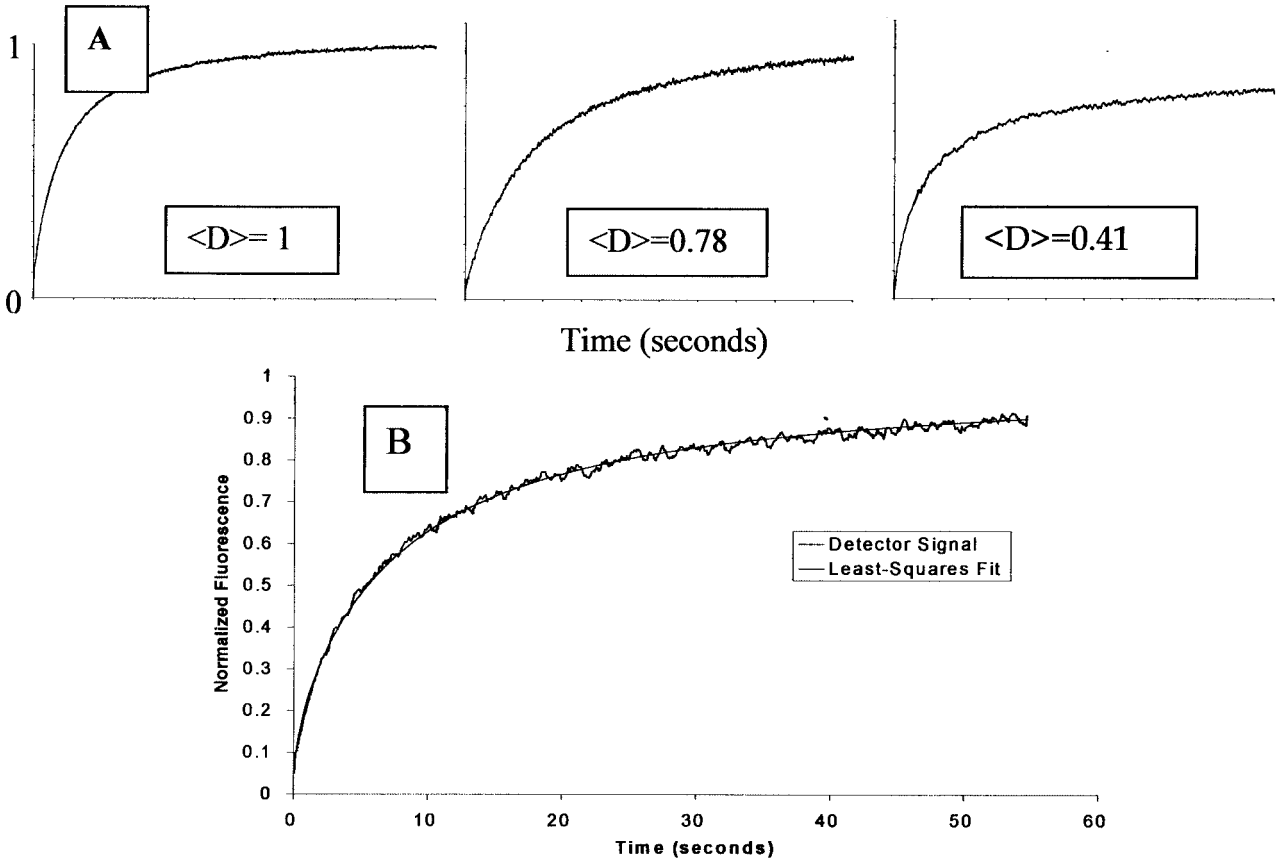

FIGURE 8 Typical FRAP recovery curves for mixtures of DLPC/DSPC containing 1 mol % NBD-PC quenched from 70°C to 25°C. (*A*) Normalized recovery curves for DSPC/DLPC bilayers containing 0%, 26%, and 50% DSPC, respectively. The diffusion coefficients shown on each curve are relative diffusion coefficients. A relative diffusion coefficient is a ratio of the diffusion coefficient measured in a system with obstacles (D) relative to the diffusion coefficient in a bulk fluid system (D_0; i.e., containing no obstacles). D_0 was measured in a fully fluid bilayer containing only DLPC and 1 mol % NBD-PC and is shown in *A*. (*B*) A typical least-squares fit to a calibration curve obtained using a sample of fluorescein in PBS buffer.

TABLE 1 Average diffusion coefficients for increasing area fractions of gel-phase lipid in bilayers containing mixtures of DLPC/DSPC and 1 mol % NBD-PC

Area fraction of gel-phase lipid (C)*	Diffusion coefficient (D)	Relative diffusion coefficient (D/D_0)
0	8.5	1
0.038	8.06	0.95
0.125	7.21	0.85
0.158	6.67	0.79
0.26	5.90	0.70
0.33	5.01	0.59
0.40	4.42	0.52
0.50	3.49	0.41
0.572	2.60	0.29
0.60	1.92	0.23
0.65	0.80	0.1
0.698	0.05	0.005

*These values are averages of at least six measurements from at least three samples; in most cases the SD was less than 3% of the recovery value. The exception is for area fractions above 55%, where the SD was below 7%.

based on the successful use of free volume models to describe solvent diffusion in three-dimensional fluids (Galla and Sackmann, 1974; Grest and Cohen, 1980, 1983). In the free-area lipid diffusion models, lipid motion is assumed to take place in several steps. Brownian motion gives rise to concentration fluctuations in the membrane leading to free areas that are devoid of lipid. When such a free area is available, an adjacent lipid can diffuse into it. This motion is assumed to take place without hindrance and at a rate dictated by D_a. The rate of lipid diffusion is then determined by the probability of finding a free area and the long-time relative diffusion coefficient is expressed by:

$$\frac{D}{D_a} = \exp(-\Delta G/RT), \tag{1}$$

where D_a is the rate with which a particle can diffuse into an available free area, R is the gas constant, and ΔG is the work required to create a target area free of other lipids. The precise value of ΔG is determined by the nature of lipid-lipid interactions and the geometry of the free areas that permit diffusion. The effects of interactions and geometry

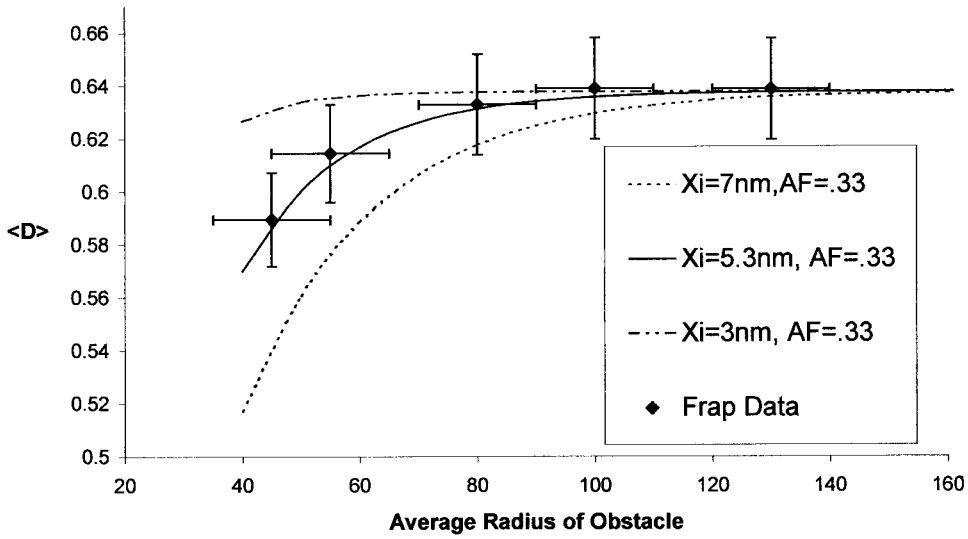

FIGURE 9 Relative diffusion coefficient $\langle D \rangle$ as a function of the domain radius R at a constant gel-phase area fraction of 33%. This graph demonstrates the strong dependence of obstructed diffusion on the obstacle size, with smaller domains being better at hindering diffusion than larger ones. The y-axis error bars are the same as shown in Fig. 8; x-axis error bars represent the 20-nm distribution in obstacle size shown in Fig. 5. The solid line is the best least-squares fit of the free-area model (at a constant value of $C = 33\%$ and graphed as $\langle D \rangle$ versus R rather than $\langle D \rangle$ versus C) to the FRAP recovery data and gives a $\xi = 5.3$ nm. The other lines show the free-area model graphed for $\xi = 7$ nm and 3 nm. Note that for domain radii larger than ~100 nm, the diffusion coefficient is no longer size dependent.

are not analytically determined but instead are often left as a free parameter that can be determined upon comparison with experiment. In most free-area models of lipid diffusion some attempt is made to relate the free parameter to specific properties of the membrane.

In 1992, Almeida et al. formalized a modified free-area model for obstructed lipid diffusion (Almeida et al., 1992a). In this model, nonpermeable areas of the membrane are modeled as disks that act as obstacles to diffusion in the plane of the bilayer. An additional modification is the addition of a soft-core repulsion between the diffusing lipids and the obstacles in the form of a boundary layer of more highly ordered fluid lipid molecules. The boundary layer modifies the available free energy and is described by a relative free-area function describing the change in free area at a distance r from an obstacle:

$$u(r) = 1 - (1 - u_0)\exp[-(r - R)/\xi], \qquad (2)$$

where u_0 is the relative free area at the boundary between obstacle and fluid phase, r is the distance from the center of the obstacle, R is the radius of the obstacle, and ξ is the coherence length over which the influence of the obstacle decays. The relative free-area functions decay as an exponential, having values ranging between one (indicating disorder) in the bulk fluid to zero (order) at the obstacle boundary. It is important to note that the parameter u_0 reflects the strength of the interaction between the obstacle and the fluid-phase molecule and should be between 0.0 and 0.5 (Almeida et al., 1992a). In the calculation of this model, it is kept constant at an intermediate value of 0.25 but plays only a small role in the final result. A local diffusion coefficient D^* can then be defined as:

$$D^*(r) = \frac{D}{D_0} = \exp\left[\left(\frac{a_s}{a_{f_0}}\right)\left(1 - \frac{1}{u(r)}\right)\right], \qquad (3)$$

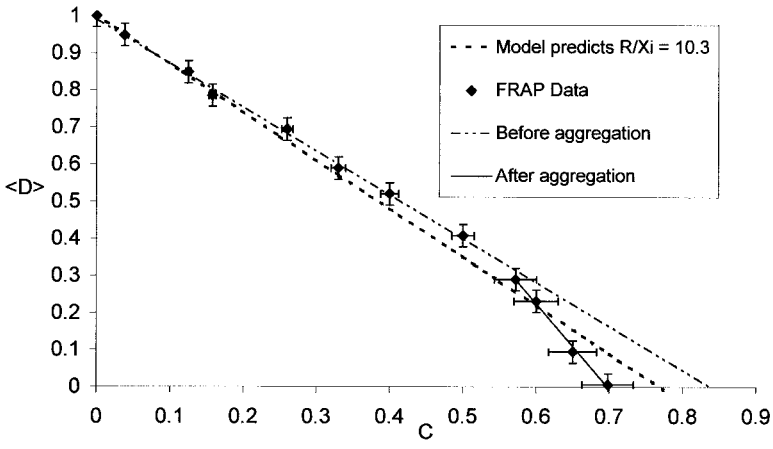

FIGURE 10 Relative diffusion coefficient $\langle D \rangle$ as a function of solid area fraction C in mixtures of DLPC/DSPC containing 1 mol % of the fluorescent probe NBD-PC. Note that although the measured diffusion coefficient goes to zero at an area fraction of ~0.70, a line drawn through the data points before $C = 0.50$ shows that without aggregation, diffusion would go to zero at an area fraction of ~0.80. The area fraction C at which long-range diffusion is abolished is the percolation threshold. The dashed line is the best least-squares fit of the free-area model to the FRAP data and gives a predicted value for R/ξ of 10.3. The data points are averages of recoveries from at least six measurements from three samples. The changing error shown in the x-axis error bars is because of increasing difficulty in accurately measuring the solid-phase area fraction at higher DSPC to DLPC ratios.

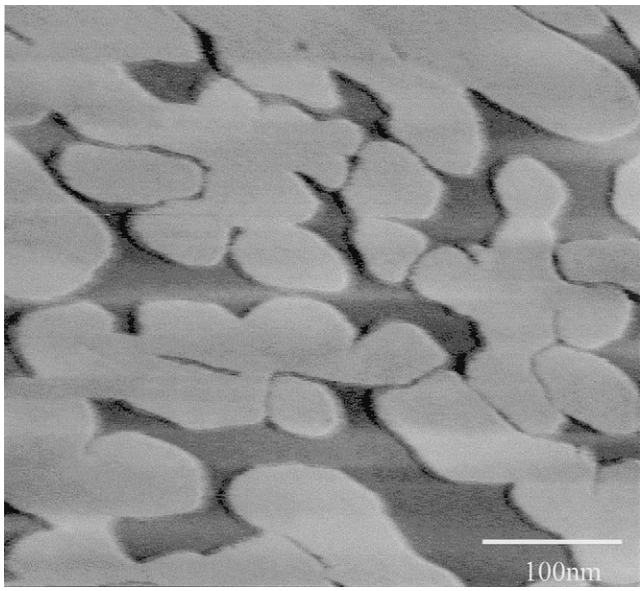

FIGURE 11 AFM subtracted height-deflection image of mica-supported DLPC/DSPC bilayers at a gel-phase area fraction near the percolation threshold. The gel-phase domains have aggregated to form more elongated domains.

where D^* is the ratio of the diffusion coefficient at a region near an obstacle (D) relative to the diffusion coefficient in the bulk fluid (D_0), a_s/a_{f0} is the ratio between the molecular area of a lipid molecule in the gel phase and the area of a lipid in the fluid phase.

To generate a long-range diffusion coefficient, the local diffusion coefficient D^* is integrated over all areas of the bilayer to produce a relationship between the long-range rate of diffusion $\langle D \rangle$, the area fraction of the solid phase obstacles (C), the size of the obstacles (R), and the coherence length over which the influence of the obstacle on the ordering of the fluid phase lipids is felt (ξ). This system of integrals has been solved numerically (Almeida et al., 1992a) and can be fit well by a second-order polynomial that depends only on R/ξ and the area fraction of the obstacles C.

Fig. 10 shows a best least-squares analysis fit of the second-order polynomial to our data and gives a value for $R/\xi = 10.3$. Because we know R, we could use this relationship to generate a ξ value; however, this would essentially be using ξ as a free parameter to fit R. We can use another tool to generate an independent ξ value to determine whether the model is accurately predicting the radius of our obstacles, namely, the relationship between obstacle size and hindrance of diffusion as shown in Fig. 9. In Fig. 10, we presented the model as $\langle D \rangle$ versus C for the value of R/ξ. Now holding C constant, we graph $\langle D \rangle$ versus R for different values of ξ and overlay our experimental $\langle D \rangle$ versus R (Fig. 9). We find that a range of ξ values between 4.5 and 6.5 nm fits our data within error. Combining this result with the previously determined $R/\xi = 10.3$ results in values of ~46–67 nm for the radius of the obstacles, a highly accurate prediction compared with the actual average obstacle radius of 60 nm. Unfortunately, theories based on thermodynamic arguments claim that the coherence length ξ should not be greater than ~2.5 nm (Jahnig, 1981). This implies that either the free-area model (inaccurately) predicts that the gel-phase domains influence the bulk fluid over a longer distance than predicted by theory or that our system is in fact displaying an unexpected long-range order.

Ordering of fluid lipid around membrane inclusions

Inclusions in bilayers lead to an increased ordering, or higher density of packing, of the fluid-phase lipids around an inclusion (Harroun et al., 1999; Heller et al., 2000; Dan and Safran, 1995; Chou et al., 2001). Thermodynamic arguments based solely on the phase transition temperature of the lipid undergoing perturbation maintain that the coherence length of the perturbation should range between 1.0 and 2.5 nm. However, it has been proposed that ordering of fluid lipids because of an inclusion is at least partially dependent on mechanical properties of the membrane such as the spontaneous monolayer curvature (fluctuations) and the bending stiffness (Dan et al., 1993, 1994). In these theoretical treatments, inclusions in membranes (such as proteins or gel-phase lipid domains) impose a thickness-matching constraint on the bilayer. The distance over which the membrane is perturbed by the inclusion can be obtained by a minimization of the bilayer energy and has the form:

$$\frac{\Delta(X)}{\Delta_0} \propto Ae^{BX}, \tag{4}$$

where X is the distance from the inclusion, Δ_0 is the value of the perturbation profile at $X = 0$, A is determined by the boundary conditions, and B is set by the molecular model describing the amphiphile making up the membrane. When B is a real number the effects on the membrane decay exponentially away from the inclusion; however, when B is a complex number, the perturbation profile will oscillate. The decay length can then extend longer than a simple exponential resulting in an extra-long coherence length, similar to what we see in our experimental system. Long-range inclusion-induced perturbations have recently been reported in giant unilamellar vesicles and were attributed to just such a mechanism (Koltover et al., 1999). In this case it was proposed that the oscillatory perturbation of the membrane resulted in the interaction of latex beads chemically adsorbed to the surface of the giant unilamellar vesicles. The interaction led to the aggregation of beads that were initially separated by at least one full bead diameter (~300–900 nm). It is possible that the long-range membrane perturbations we see in our phase-separated system

are also caused by local elastic deformations of the membrane imposed by the presence of the gel-phase domains. Additional studies determining, for example, how coherence length scales with membrane properties such as bending stiffness, will be necessary to establish whether or not membrane fluctuations are indeed responsible for the unexpectedly long coherence length.

CONCLUSIONS

Fluid lipid bilayers of DLPC containing gel-phase DSPC domains were formed on mica and analyzed using AFM and FRAP. The gel-phase domains are roughly centrosymmetric and increase in number with increasing area fraction. Aggregation of the gel-phase domains at higher area fractions results in the disconnection of the fluid phase at an area fraction of ~70% (the percolation threshold; fluorescence recovery is also abolished at this area fraction). We found that lateral lipid diffusion is obstructed by the presence of the gel-phase domains and is dependent on the size, shape, and area fraction of the solid-phase domains. A free-area model formalized by Almeida et al. resulted in accurate predictions of the obstacle-dependent diffusion coefficient and gel-phase domain size. The results show that smaller obstacles are more efficient at blocking diffusion than larger ones, in keeping with previously reported Monte Carlo simulations, and that the size dependency is nullified for obstacles that possess radii larger than 100 nm. Additionally, diffusion decreases with decreasing compactness of obstacles and with increasing area fraction, as predicted. Fitting the free-area model to our data displayed an unexpected long-range membrane perturbation, previously seen experimentally, but with a few noted exceptions, not yet predicted theoretically.

We thank Michael Saxton and Dan Axelrod for helpful discussions and Chad Leidy for providing the preliminary research that led to this paper.

This work was supported in part by the MRSEC Program of the National Science Foundation under award DMR-9808677 and a Whitaker Foundation Biomedical Engineering grant. M.L.L. acknowledges the generous gift of Joe and Essie Smith for endowing part of this work.

REFERENCES

Abney, J. R., and B. A. Scalettar. 1995. Fluctuations and membrane heterogeneity. *Biophys. Chem.* 57:27–36.

Abney, J. R., B. A. Scalettar, and J. C. Owicki. 1989. Mutual diffusion of interacting membrane proteins. *Biophys. J.* 56:315–326.

Almeida, P. F. F., W. L. C. Vaz, and T. E. Thompson. 1992a. Lateral diffusion and percolation in 2-phase, 2-component lipid bilayers: topology of the solid-phase domains in-plane and across the lipid bilayer. *Biochemistry.* 31:7198–7210.

Almeida, P. F. F., W. L. C. Vaz, and T. E. Thompson. 1992b. Lateral diffusion in the liquid phases of dimyristoylphosphatidylcholine cholesterol lipid bilayers: a free volume analysis. *Biochemistry.* 31: 6739–6747.

Axelrod, D., D. E. Koppel, J. Schlessinger, E. Elson, and W. W. Webb. 1976. Mobility measurement by analysis of fluorescence photobleaching recovery kinetics. *Biophys. J.* 16:1055–1069.

Balcom, B. J., and N. O. Petersen. 1993. Lateral diffusion in model membranes is independent of the size of the hydrophobic region of molecules. *Biophys. J.* 65:630–637.

Balgavy, P., M. Dubnickova, N. Kucerka, M. A. Kiselev, S. P. Yaradaikin, and D. Uhrikova. 2001. Bilayer thickness and lipid interface area in unilamellar extruded 1,2-diacylphosphatidylcholine liposomes: a small-angle neutron scattering study. *Biochim. Biophys. Acta. Biomembr.* 1512:40–52.

Berryman, J. G. 1983. Random close packing of hard spheres and disks. *Phys. Rev. A.* 27:1053–1061.

Brown, D. A., and E. London. 2000. Structure and function of sphingolipid- and cholesterol-rich membrane rafts. *J. Biol. Chem.* 275: 17221–17224.

Bussell, S. J., D. A. Hammer, and D. L. Koch. 1994. The effect of hydrodynamic interactions on the tracer and gradient diffusion of integral membrane proteins in lipid bilayers. *J. Fluid Mech.* 258:167–190.

Bussell, S. J., D. L. Koch, and D. A. Hammer. 1995. Effect of hydrodynamic interactions on the diffusion of integral membrane proteins: tracer diffusion in organelle and reconstituted membranes. *Biophys. J.* 68: 1828–1835.

Cherry, R. J., P. R. Smith, I. E. G. Morrison, and N. Fernandez. 1998. Mobility of cell surface receptors: a re-evaluation. *FEBS Lett.* 430: 88–91.

Chou, T., K. S. Kim, and G. Oster. 2001. Statistical thermodynamics of membrane bending-mediated protein-protein attractions. *Biophys. J.* 80: 1075–1087.

Dan, N., A. Berman, P. Pincus, and S. A. Safran. 1994. Membrane-induced interactions between inclusions. *J. Phys. II.* 4:1713–1725.

Dan, N., P. Pincus, and S. A. Safran. 1993. Membrane-induced interactions between inclusions. *Langmuir.* 9:2768–2771.

Dan, N., and S. A. Safran. 1995. Solubilization of proteins in membranes. *Isr. J. Chem.* 35:37–40.

de Almeida, R. F. M., L. M. S. Loura, A. Fedorov, and M. Prieto. 2002. Nonequilibrium phenomena in the phase separation of a two-component lipid bilayer. *Biophys. J.* 82:823–834.

Ditaranto, K., T. L. Tekirian, and A. J. Yang. 2001. Lysosomal membrane damage in soluble A beta-mediated cell death in Alzheimer's disease. *Neurobiol. Dis.* 8:19–31.

Dodd, T. L., D. A. Hammer, A. S. Sangani, and D. L. Koch. 1995. Numerical simulations of the effect of hydrodynamic interactions on diffusivities of integral membrane proteins. *J. Fluid Mech.* 293:147–180.

Eze, M. O. 1992. Membrane fluidity, reactive oxygen species, and cell-mediated immunity: implications in nutrition and disease. *Med. Hypotheses.* 37:220–224.

Feder, T., I. Brust-Mascher, J. Slattery, B. Baird, and W. Webb. 1996. Constrained diffusion or immobile fraction on cell surfaces: a new interpretation. *Biophys. J.* 70:2767–2773.

Galla, H. J., and E. Sackmann. 1974. Lateral mobility of pyrene in model membranes of phospholipids with different chain length. *Ber. Bunsenges. Phys. Chemie* 78:949–953.

Garver, T. D., Q. Ren, S. Tuvia, and V. Bennett. 1997. Tyrosine phosphorylation at a site highly conserved in the L1 family of cell adhesion molecules abolishes ankyrin binding and increases lateral mobility of neurofascin. *J. Cell Biol.* 137:703–714.

Gheber, L. A., and M. Edidin. 1999. A model for membrane patchiness: lateral diffusion in the presence of barriers and vesicle traffic. *Biophys. J.* 77:3163–3175.

Giocondi, M. C., V. Vie, E. Lesniewska, P. E. Milhiet, M. Zinke-Allmang, and C. Le Grimellec. 2001. Phase topology and growth of single domains in lipid bilayers. *Langmuir.* 17:1653–1659.

Gorter, E., and F. Grendel. 1925. On biomolecular layers of lipoids on the chromocytes of the blood. *J. Exp. Med.* 41:439–443.

Grest, G. S., and M. H. Cohen. 1980. Liquid-glass transition: dependence of the glass transition on heating and cooling rates. *Phys. Rev. B.* 21:4113–4117.

Grest, G. S., and M. H. Cohen. 1983. Percolation and the glass transition. *Ann. Isr. Phys. Soc.* 5:187–206.

Harroun, T. A., W. T. Heller, T. M. Weiss, L. Yang, and H. W. Huang. 1999. Experimental evidence for hydrophobic matching and membrane-mediated interactions in lipid bilayers containing gramicidin. *Biophys. J.* 76:937–945.

Heller, W. T., A. J. Waring, R. I. Lehrer, T. A. Harroun, T. M. Weiss, L. Yang, and H. W. Huang. 2000. Membrane thinning effect of the beta-sheet antimicrobial protegrin. *Biochemistry.* 39:139–145.

Ho, C., B. W. Williams, and C. D. Stubbs. 1992. Analysis of cell membrane micro-heterogeneity using the fluorescence lifetime of DPH-type fluorophores. *Biochim. Biophys. Acta.* 1104:273–282.

Hollars, C. W., and R. C. Dunn. 1997. Submicron fluorescence, topology, and compliance measurements of phase-separated lipid monolayers using tapping-mode near-field scanning optical microscopy. *J. Phys. Chem. B.* 101:6313–6317.

Hollars, C. W., and R. C. Dunn. 1998. Submicron structure in L-α-dipalmitoylphosphatidylcholine monolayers and bilayers probed with confocal, atomic force, and near-field microscopy. *Biophys. J.* 75: 342–353.

Jahnig, F. 1981. Critical effects from lipid-protein interaction in membranes. I. Theoretical description. *Biophys. J.* 36:329–345.

Johnson, M., D. Berk, D. Blankschtein, D. Golan, R. Jain, and R. Langer. 1996. Lateral diffusion of small compounds in human stratum corneum and model lipid bilayer systems. *Biophys. J.* 71:2656–2668.

Koltover, I., J. O. Radler, and C. R. Safinya. 1999. Membrane mediated attraction and ordered aggregation of colloidal particles bound to giant phospholipid vesicles. *Phys. Rev. Lett.* 82:1991–1994.

Korlach, J., P. Schwille, W. W. Webb, and G. W. Feigenson. 1999. Characterization of lipid bilayer phases by confocal microscopy and fluorescence correlation spectroscopy. *Proc. Natl. Acad. Sci. U.S.A.* 96:8461–8466.

Kucik, D. F., E. L. Elson, and M. P. Sheetz. 1999. Weak dependence of mobility of membrane protein aggregates on aggregate size supports a viscous model of retardation of diffusion. *Biophys. J.* 76:314–322.

Ladha, S. 1998. Lipid heterogeneity and membrane fluidity in a highly polarized cell, the mammalian spermatozoon. *J. Membr. Biol.* 165:1–10.

Lee, S. B., and S. Torquato. 1990. Monte-Carlo study of correlated continuum Percolation: universality and percolation thresholds. *Phys. Rev. A.* 41:5338–5344.

Martins, J., and E. Melo. 2001. Molecular mechanism of lateral diffusion of py10-PC and free pyrene in fluid DMPC bilayers. *Biophys. J.* 80: 832–840.

McKiernan, A. E., R. I. MacDonald, R. C. MacDonald, and D. Axelrod. 1997. Cytoskeletal protein binding kinetics at planar phospholipid membranes. *Biophys. J.* 73:1987–1998.

McKiernan, A. E., T. V. Ratto, and M. L. Longo. 2000. Domain growth, shapes, and topology in cationic lipid bilayers on mica by fluorescence and atomic force microscopy. *Biophys. J.* 79:2605–2615.

Mesquita, R., E. Melo, T. E. Thompson, and W. L. C. Vaz. 2000. Partitioning of amphiphiles between coexisting ordered and disordered phases in two-phase lipid bilayer membranes. *Biophys. J.* 78: 3019–3025.

Minton, A. 1989. Lateral diffusion of membrane proteins in protein-rich membranes: a simple hard particle model for concentration dependence of the two- dimensional diffusion coefficient. *Biophys. J.* 55:805–808.

O'Toole, P. J., C. Wolfe, S. Ladha, and R. J. Cherry. 1999. Rapid diffusion of spectrin bound to a lipid surface. *Biochim. Biophys. Acta. Biomembr.* 1419:64–70.

Owen, J. S. 1990. Extrahepatic cell membrane lipid abnormalities and cellular dysfunction in liver disease. *Drugs.* 40:73–83.

Periasamy, N., and A. S. Verkman. 1998. Analysis of fluorophore diffusion by continuous distributions of diffusion coefficients: application to photobleaching measurements of multicomponent and anomalous diffusion. *Biophys. J.* 75:557–567.

Picard, F., M.-J. Paquet, E. J. Dufourc, and M. Auger. 1998. Measurement of the lateral diffusion of dipalmitoylphosphatidylcholine adsorbed on silica beads in the absence and presence of melittin: a ^{31}P two-dimensional exchange solid-state NMR study. *Biophys. J.* 74:857–868.

Pink, D. A., D. J. Laidlaw, and D. M. Chisholm. 1986. Protein lateral movement in lipid bilayers: Monte Carlo simulation studies of its dependence upon attractive protein-protein interactions. *Biochim. Biophys. Acta.* 863:9–17.

Sako, Y., and A. Kusumi. 1995. Barriers for lateral diffusion of transferrin receptor in the plasma membrane as characterized by receptor dragging by laser tweezers: fence versus tether. *J. Cell Biol.* 129:1559–1574.

Saxton, M. J. 1989. Lateral diffusion in an archipelago: distance dependence of the diffusion coefficient. *Biophys. J.* 56:615–622.

Saxton, M. J. 1990. Lateral diffusion in a mixture of mobile and immobile particles: a Monte-Carlo study. *Biophys. J.* 58:1303–1306.

Saxton, M. J. 1992. Lateral diffusion and aggregation: a Monte-Carlo study. *Biophys. J.* 61:119–128.

Saxton, M. J. 1994. Anomalous diffusion due to obstacles: a Monte Carlo study. *Biophys. J.* 66:394–401.

Saxton, M. J. 1997. Single-particle tracking: the distribution of diffusion coefficients. *Biophys. J.* 72:1744–1753.

Scalettar, B. A., and J. R. Abney. 1991. Molecular crowding and protein diffusion in biological membranes. *Comments Mol. Cell Biophys.* 7:79–107.

Schram, V., H. N. Lin, and T. E. Thompson. 1996. Topology of gel-phase domains and lipid mixing properties in phase-separated two-component phosphatidylcholine bilayers. *Biophys. J.* 71:1811–1822.

Schram, V., J. F. Tocanne, and A. Lopez. 1994. Influence of obstacles on lipid lateral diffusion: computer simulation of FRAP experiments and application to proteoliposomes and biomembranes. *Eur. Biophys. J.* 23:337–348.

Schwille, P., J. Korlach, and W. W. Webb. 1999. Fluorescence correlation spectroscopy with single-molecule sensitivity on cell and model membranes. *Cytometry.* 36:176–182.

Simson, R., B. Yang, S. E. Moore, P. Doherty, F. S. Walsh, and K. A. Jacobson. 1998. Structural mosaicism on the submicron scale in the plasma membrane. *Biophys. J.* 74:297–308.

Singer, S. J., and G. L. Nicholson. 1972. The fluid mosaic model of the structure of cell membranes. *Science.* 175:720–721.

Soumpasis, D. M. 1983. Theoretical analysis of fluorescence photobleaching recovery experiments. *Biophys. J.* 41:95–97.

Tocanne, J. F., L. Cezanne, A. Lopez, B. Piknova, V. Schram, J. F. Tournier, and M. Welby. 1994. Lipid domains and lipid protein interactions in biological membranes. *Chem. Phys. Lipids.* 73:139–158.

Vaz, W. L. C. 1992. Translational diffusion in phase separated lipid bilayer systems. *Comments Mol. Cell. Biophys.* 8:17–36.

Vaz, W. L. C., D. Hallmann, R. M. Clegg, A. Gambacorta, and M. De Rosa. 1985. A comparison of the translational diffusion of a normal and a membrane-spanning lipid in L_A phase 1-palmitoyl-2-oleoylphosphatidylcholine bilayers. *Eur. Biophys. J.* 12:19–24.

Webb, W. W., L. S. Barak, D. W. Tank, and E.-S. Wu. 1981. Molecular mobility on the cell surface. *Biochem. Soc. Symp.* 46:191–205.